JOURNAL OF MATERIALS SCIENCE 26 (1991) 3503–3510

Nanocomposites in mullite–ZrO_2 and mullite–TiO_2 systems synthesised through alkoxide hydrolysis gel routes: microstructure and fractography

Ph. COLOMBAN*
Groupe de Chimie du Solide, LPMC-U.A.1254 (CNRS), Ecole Polytechnique, 91128 Palaiseau, France

L. MAZEROLLES
Laboratoire de Chimie Appliquée de l'Etat Solide, CECM-CNRS, 15 rue Georges Urbain, 94400 Vitry sur Seine, France

The sol–gel process allows preparation of very homogeneous and reactive monolithic, optically clear gels. Low-temperature thermal treatments (700–1000 °C) lead to amorphous optically clear samples ("glass"). Amorphous mullite compositions ($0.4Al_2O_3$–$0.6SiO_2$ to $0.8Al_2O_3$–$0.2SiO_2$) retain large amounts of Ti and Zr elements. The crystallization has been studied by differential thermal analysis, dilatometry, X-ray and electron diffraction and Raman scattering. The nucleation begins above 1000 °C with the departure of the last protonic species, the amorphous matrix being completely crystallized only above 1400 °C. The addition of Zr and Ti elements leads to a homogeneous nucleation of phases with a composition close to ZrO_2 and $Al_2Ti_3O_9$ (EDX analysis) above the solubility limit. TEM and SEM analyses show that the precipitate size remains submicrometric over a wide temperature range (1000–1400 °C) and consequently glass-like mechanical properties, as well as toughening effects, caused by the presence of nanoprecipitates, are observed.

1. Introduction

During the last decade, the need for new materials and new forming methods has become increasingly clear. One of the emerging processes in the ceramic field is the use of sol–gel routes [1, 2]. Sol–gel processes allow the preparation of very homogeneous and reactive gels, either in the form of fine powder or directly in the form of optically clear monoliths. Low-temperature thermal treatments (700–1000 °C) lead to dense amorphous materials, with an aspect like a glass. Heating at higher temperature generally induces crystallization before melting. In this paper, we discuss only the behaviour of monoliths prepared by very slow hydrolysis (more than several weeks). This route is not well suited to most applications, but we can thus reach the optimum that the ceramic art could obtain with powder routes, but after optimization of many parameters. This means of preparing monoliths is thus an interesting exploratory investigation.

In previous work [3–6] we have demonstrated that optimized sol–gel routes lead to submicronic optically translucent (clear) amorphous or crystalline mullite, with an intermediate glass-ceramic state which is observed in the 1000–1400 °C temperature range. This behaviour is often encountered for sol–gel ceramics, in association with the presence of a phase unobserved in the usual phase diagrams. Furthermore, it was shown that these glass-ceramics exhibit a high microhardness, related to the ratio of submicronic precipitates [2].

A few years ago, mineralogists showed that mullite could dissolve elements such as Fe, Ti, or even Zr, but this solubility drastically decreased with temperature [7–9]. Thus, it was attractive to use the limit of solubility as a source of a homogeneous nucleation of ZrO_2 and TiO_2 particles in a mullite matrix. It was quickly pointed out that mullite–ZrO_2 composites lead to a significant improvement in toughness and strength over pure mullite. However, these composites generally have a large microstructure ($\geq$ 2–5 μm) [10–12].

2. Experimental procedure

2.1. Samples

The synthesis of mullite optically clear monolithic gel has been previously described [3, 4] and we give here only a brief report. A hexane solution of aluminium sec-butoxide and silicon methoxide (Fluka or Dynasyl) is slowly hydrolysed with atmospheric moisture by the gas invasion through the bottle stopper. Hydrolysis time is typically 6 months, which assures a

* *Present address*: ONERA, BP72 92322 Chatillon, France.

0022–2461/91 $03.00 + .12 © *1991 Chapman and Hall Ltd.*

very good homogeneity (and transparency of gel). In the same time, evolution of solvents and products of the hydrolysis polycondensation (hexane, butanol, methanol) occurs

$$M(OR)_n + nH_2O \rightarrow M(OH)_n + nROH \quad (1)$$

$$M(OH)_n \rightarrow MO_{n/2} + n/2\,H_2O \quad (2)$$

After that, we obtain an optically clear monolith (about 10–12 cm^3) of mullite gel (Fig. 1). The composition of the gel is close to $3Al_2O_3 \cdot 2SiO_2 \cdot 14H_2O$.

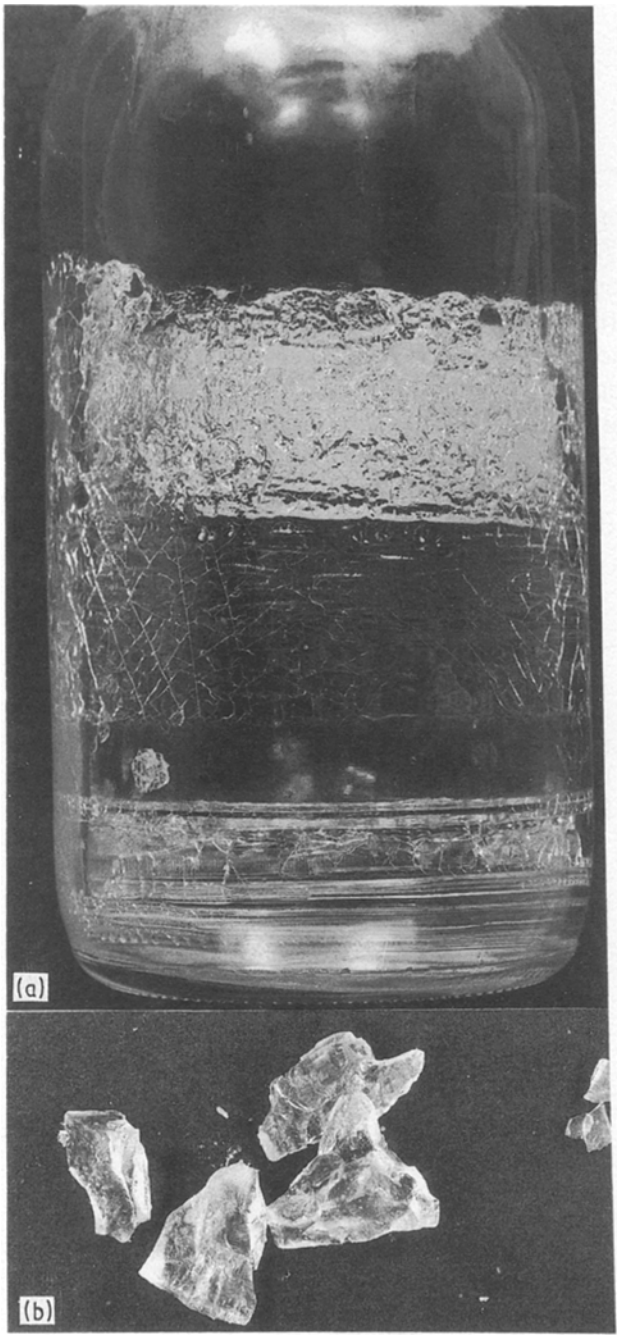

Figure 1 (a): Monolithic "mullite–TiO_2" gel in its bottle. A cracked film formed at the inner surface gives a picture of the solution level before hydrolysis (the hexane alkoxide solution filled half the bottle). The resulting monolith is at the bottom (thickness 10 mm, diameter 40 mm). Cracks are visible at the monolith surface. These samples were dried at 80 °C. (b) Optically clear monoliths (mullite–ZrO_2) after heating for 4 days at 1000 °C (mean size 10 mm × 3 mm × 5 mm).

Introduction of titanium ethoxide or zirconium *n*-propoxide in the alkoxide–hexane solution allows the preparation of Ti- and Zr-modified compositions. The prepared samples discussed here have compositions (mol) close to 0.8 mullite (3/2)–0.2ZrO_2 (or TiO_2). Heating above 500 °C transforms the gel into an optically clear, amorphous but porous glass with about 35%–40% weight loss, corresponding to the loss of water (and alcohol traces) filling the porous polymeric gel structure, and of some of the OH^- groups resulting from the hydrolysis–polycondensation.

However, the weight loss continues up to 1000 °C (< 1%), because the last OH^- defects are only eliminated on the complete crystallization [13]. After this thermal treatment, the gel breaks in smaller pieces (Fig. 1b) but remains optically clear up to 1100 °C. It becomes opalescent at higher temperature and white above 1300 °C for Zr- and Ti-containing compositions. Pure mullite monoliths remain optically clear up to 1500 °C [4]. All thermal treatments were done in air.

2.2. Techniques

X-ray powder diagrams are recorded using λCuK_α radiation. DTA traces were obtained with a Dupont de Nemours instrument between 25 and 1500 °C. Dilatometry was performed with an Instrument S.A. Àdamel D124 apparatus. Micro-Raman spectra were recorded with an Instrument S.A. Mole Microprobe using a 1.5 W argon ion laser of Spectra Physics, the 514.5 nm excitation line being used to shift the fluorescence, often encountered with samples heated below 700 °C.

TEM observations were performed from powders on a Jeol 2000FX electron microscope at 200 kV. This microscope is equipped with an energy X-ray dispersive spectrometer (Tracor) for chemical analysis (Si(Li) detector). Fractography studies were achieved on an SEM Zeiss DSM950.

3. Results and discussion

3.1. Formation of orthorhombic mullite from gel

The formation of mullite through various methods (solid state reactions from kaolin or from ball-milled amorphous or crystalline oxides, sol–gel routes, etc.) have been extensively studied (see, for instance, [13–18]). The structure of the mullite "glass" as well as the nature of the phases occurring before the formation of the orthorhombic mullite have been discussed. In fact, from the micronic scale heterogeneous mixing of oxide powders to the "molecular" mixing achieved in gel, the size of local inhomogeneities decreases and thus the temperature of sintering (and of phase formation) can be lowered. The structure of mullite is constituted by an association of octahedral chains linked by tetrahedra chains, with Al and Si disordered atoms on centres of tetrahedra. The non-stoichiometry is related with the Al/Si ratio inducing orientational tetrahedra

disorder [4, 7]. Owing to this structure, the phase diagram is very sensitive to the method of synthesis.

Fig. 2 shows the phase diagram that we have established on the basis of X-ray diagrams, Raman scattering and electron diffraction spectra and EDX analysis for materials prepared by the slow hydrolysis route [6]. We observe a large amorphous domain and the presence of disordered mullite phase ("tetragonal mullite") in an amorphous mullite matrix. As is usually encountered for sol–gel prepared compositions, similarities exist with the features observed for quenched materials [3, 4, 19]. This can be related to the fact that sol–gel polycondensation is also a means of synthesis from a liquid state to a solid state.

We have previously shown [3–6] that below 1000 °C a "mullite glass" can be obtained, at least between $3Al_2O_3$–$7SiO_2$ and $8Al_2O_3$–$2SiO_2$. At about 1000 °C a strong shrinkage takes place (Fig. 3) and an intense DTA exothermic peak is simultaneously observed. Material exhibits broader X-ray powder patterns than the usual γ-Al_2O_3 (spinel) phase ones.

However, vibrational spectroscopy and EDX microanalysis indicate that both amorphous and spinel-like phases have a non-stoichiometric mullite composition (at least between $4.5Al_2O_3$–$5.5SiO_2$ and $7Al_2O_3$–$3SiO_2$). No amorphous SiO_2 or alumina-rich spinel phases are detected as claimed by some authors*. The nucleation of mullite begins after the DTA peak and is finished between 1300 and 1400 °C, as a function of composition. This nucleation is correlated with the loss of the last OH^- defects [13]. The role of OH^- groups in the formation of mullite phase was previously underlined by Brown *et al.* [20], in the case of kaolinite–mullite transformation. The importance of OH^- groups on densification can be related to the structure relationship: spinel-like structure contains a large amount of vacancies ([V]) and the γ-Al_2O_3 phase is stabilized by the protons. Mullite structure is based on the following equilibrium:

$$2Si + O \rightleftharpoons 2Al + [V] \qquad (3)$$

inducing many vacancies and, hence, OH^- potential locations. The critical influence of OH^- defects in the nucleation of some phases was also observed for TiO_2 (a high content favours the formation of brookite) [21, 22].

In our case, complete crystallization was only observed after thermal treatment at 1400 °C [3–6, 18]. Between 1000 and 1400 °C the material is a glassy mullite/crystalline mullite composite and some of its properties are imposed by the glassy part (e.g. fracture behaviour [5, 6]) even if X-ray patterns reveal perfectly crystallized species.

The final crystallization of the "glassy" matrix is visible on dilatometric traces with the last "1300 °C step" and sometimes on DTA traces with an anomaly of the base line. Note that monoliths remain optically clear up to 1500 °C. We notice that, below 1400 °C, the ceramic microstructure is only temperature dependent (no time dependence). At this temperature the grain size is typically 1 μm × 0.4 μm × 0.05 μm. No porosity is observed and the samples may be considered fully

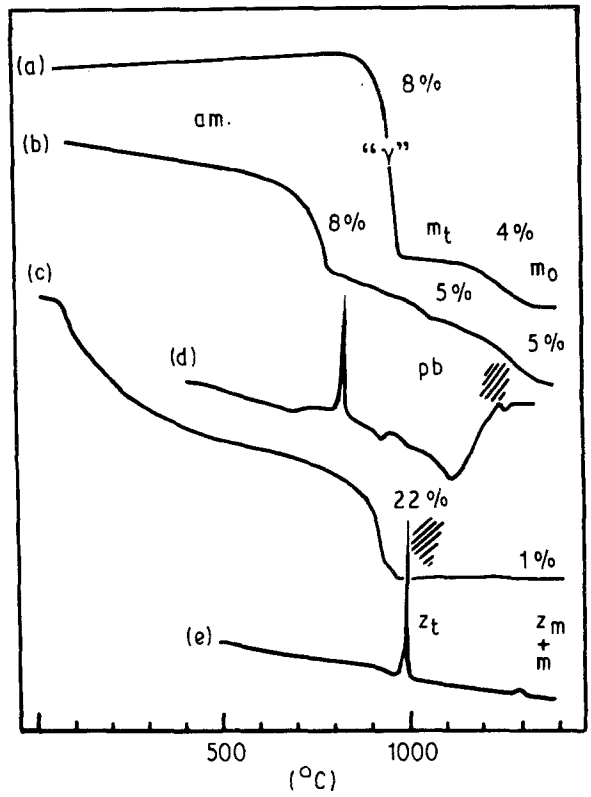

Figure 3 Dilatometric (a, b, c) and differential thermal analysis (d, e) traces recorded for: (a) pure $3Al_2O_3$–$2SiO_2$ mullite gel after a previous heating at 500 °C, 4 h; (b, d) mullite–TiO_2($3Al_2O_3$–$2SiO_2$–$0.25TiO_2$) (c, e) mullite–ZrO_2($3Al_2O_3$–$2SiO_2$–$0.25ZrO_2$). The shrinkage (%) is given versus initial length. The main structural states are given: amorphous (am), rutile traces (R), pseudo-brookite (pb), tetragonal zirconia (Zt), monoclinic zirconia (Zm). The other symbols are in Fig. 2. Cross-hatched area indicates the transition from optical clearness to translucence.

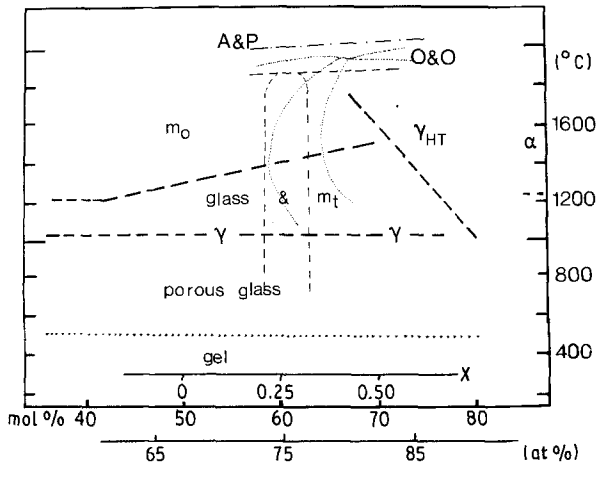

Figure 2 Al_2O_3–SiO_2 phase diagram for materials prepared by sol–gel slow hydrolysis route [6]. Phases are obtained on heating. (—) Rough limit between phases: gel, porous glass, "γ" spinel-like disordered phase, tetragonal (m_t) and orthorhombic (m_o) mullite, α alumina, "γ_{HT}" high-temperature spinel phase. Phase diagrams previously established by (–·–, – – –) Aksay and Pask (AP) [9] and (· · · ·) Okada and Otsuka (O) [16, 17] are indicated. Concentrations are given in mol % Al_2O_3, in at % Al and by the x deviation to Cameron's formula ($Al_2Al_{2+2x}Si_{2-2x}O_{10-x}$).

* An alumina-rich spinel phase (γ_{HT}) is observed after high-temperature annealing for $x \geq 0.4$ composition. Si traces stabilize this structure.

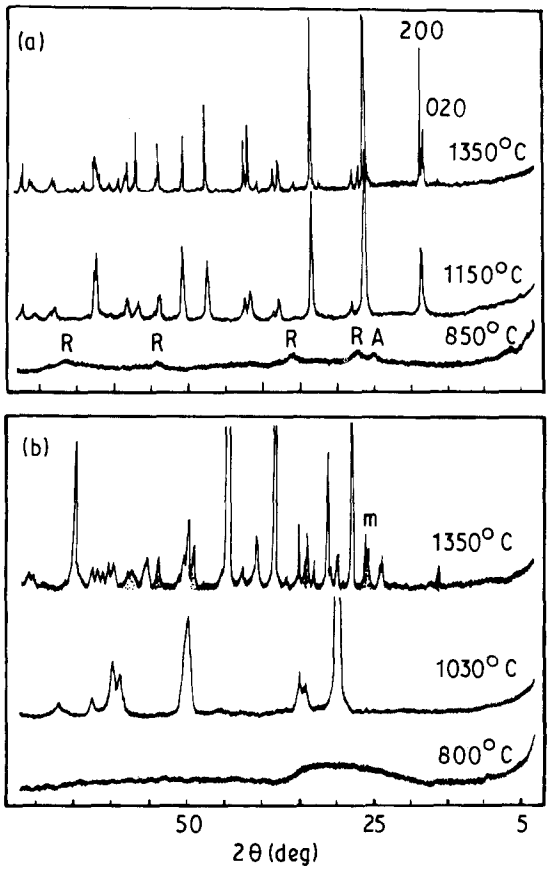

Figure 4 X-ray powder diagram (λ CuK_α) of (a) mullite–TiO_2 and (b) mullite–ZrO_2 heated at various temperatures (4–5 days). A: anatase trace, R: rutile time.

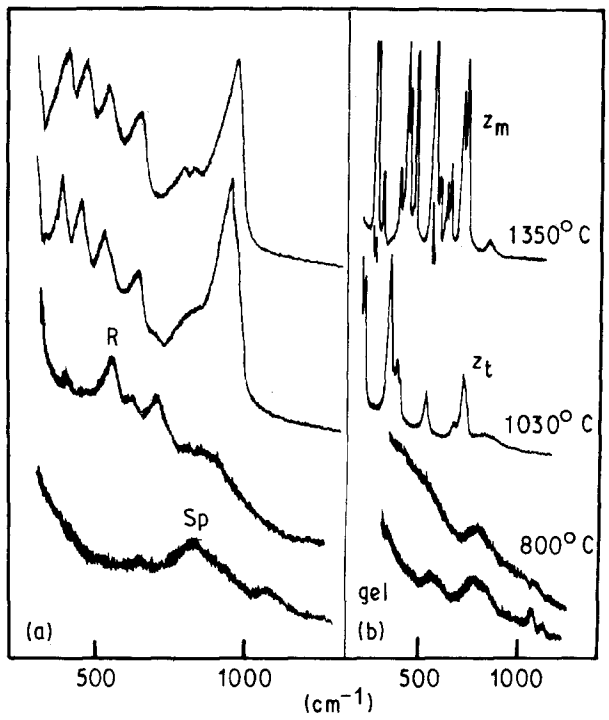

Figure 5 Raman spectra of (a) mullite–TiO_2 and (b) mullite–ZrO_2 heated at various temperatures (4–5 days).

dense even the microhardness is maximum above 1600 °C [13].

3.2. Mullite–ZrO_2 and mullite–TiO_2 glasses

Addition of Zr in large amounts (up to 20 mol %) does not reduce the stability domain of the "glassy" mullite form, at least in the range from $4Al_2O_3$–$6SiO_2$ to $8Al_2O_3$–$2SiO_2$. Samples remain optically clear (Fig. 1a) and typically amorphous X-ray powder diagrams are observed. The Raman spectrum (Fig. 5b) is similar to that of the gel and agrees with a spinel-like structure (broad peak at 770 cm^{-1}) [3, 4]. As the Raman scattering of zirconia is very intense, whereas that of spinel-like material is very poor, it is possible to affirm, from the spectra in Fig. 5, that all Zr is dissolved in the glass.

For mullite–Ti glass (Fig. 5a) we see that after thermal treatment at 800 °C, Raman scattering of Ti-containing samples shows a broad spectrum typical of a disordered spinel structure (Sp) with additional weak bands of rutile phase (235, 440, 610 cm^{-1}) (R) [24, 25]. In this case the low intensity of the spectra due to TiO_2 phase indicates that only traces of rutile are present. An SEM study confirmed the absence of visible precipitates to a resolution of 10 nm.

Dilatometric traces of monoliths with ~ 5% TiO_2 are an intermediate case between the pure mullite one and traces on Fig. 3b: the shrinkage occurs in three steps at 950, 1180 and 1380 °C.

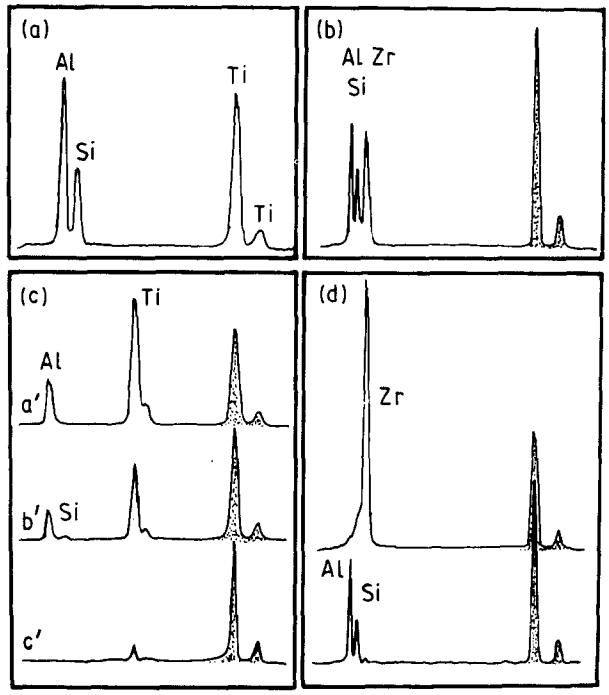

Figure 6 EDX microanalysis of (a, c) mullite–TiO_2 and (b, d) mullite–ZrO_2. (a) Crystallized nanocomposites heated 1 week at 1150 °C (probe size is about 100 times larger than precipitate size). After heating for 1 week at 1350 °C, precipitation of $Al_2Ti_3O_9$ (crystalline form a', amorphous form b') and of TiO_2 traces (c'), amorphous phase is observed for Ti-containing samples (c), whereas ZrO_2 precipitates (d) are observed in Zr-containing monoliths. Note that, in some places, poorly crystallized mullite samples contain Zr traces (dotted peak: Cu element of the grid),

3.3. Nucleation in mullite–ZrO_2 and mullite–TiO_2 materials

As shown in the X-ray powder patterns (Fig. 4) and Raman spectra (Fig. 5), nucleation of the crystalline

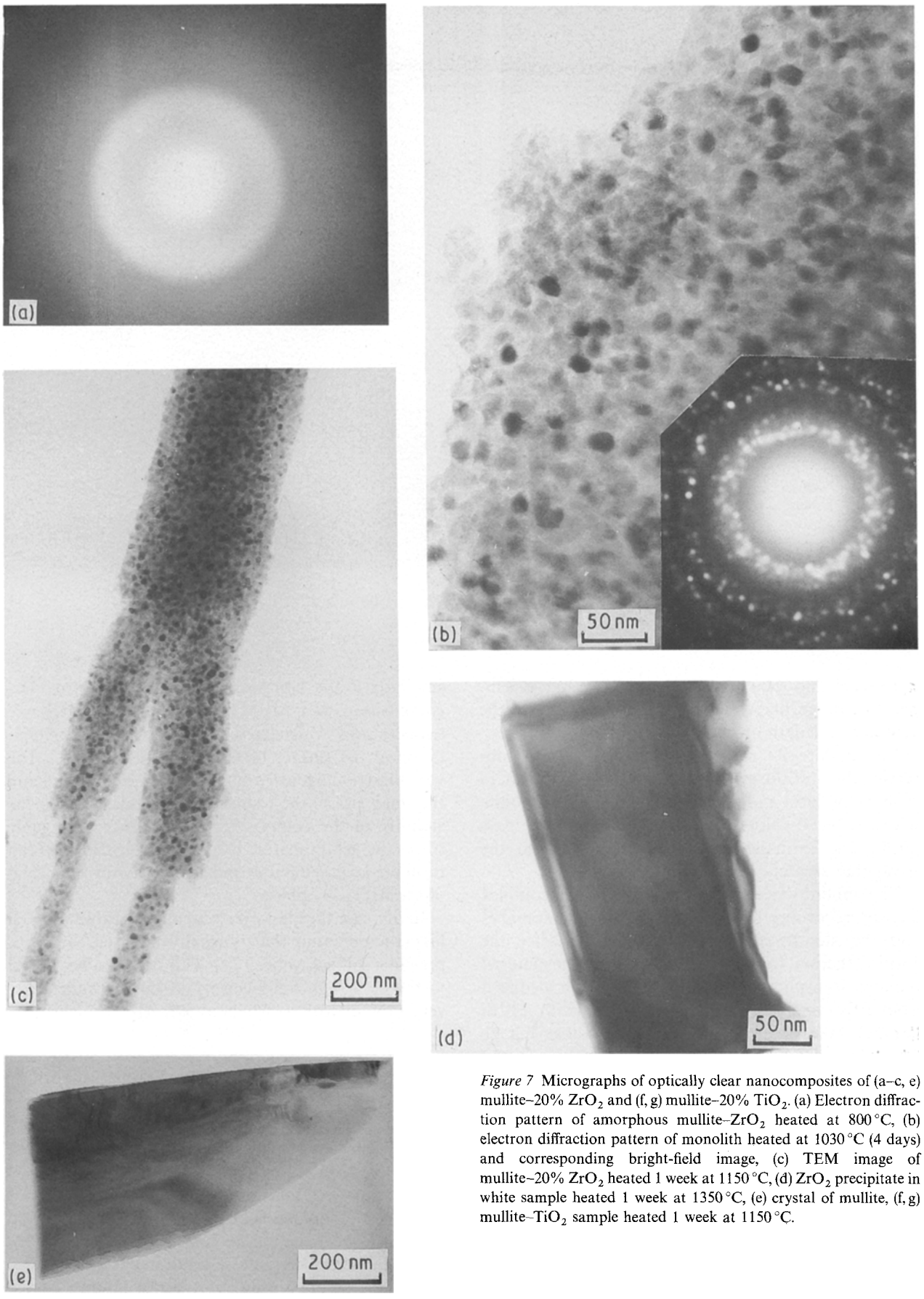

Figure 7 Micrographs of optically clear nanocomposites of (a–c, e) mullite–20% ZrO_2 and (f, g) mullite–20% TiO_2. (a) Electron diffraction pattern of amorphous mullite–ZrO_2 heated at 800 °C, (b) electron diffraction pattern of monolith heated at 1030 °C (4 days) and corresponding bright-field image, (c) TEM image of mullite–20% ZrO_2 heated 1 week at 1150 °C, (d) ZrO_2 precipitate in white sample heated 1 week at 1350 °C, (e) crystal of mullite, (f, g) mullite–TiO_2 sample heated 1 week at 1150 °C.

phase occurs at about 850 and 1000 °C for Ti- and Zr-added compositions, respectively. Tetragonal zirconia and a new phase, for Ti-containing materials, are observed. The relatively low intensity of Raman spectra indicates that the amorphous part remains very large up to 1200–1300 °C, which is confirmed by coupled electronic diffraction and EDX analysis (Fig. 6). Fig. 7 shows micrographs of optically clear monoliths obtained after heating 4 days at 1030 °C (mullite–ZrO_2) and 1150 °C (mullite–TiO_2). We observe a very homogeneous distribution of ovoid particles in a glassy matrix. These monoliths become

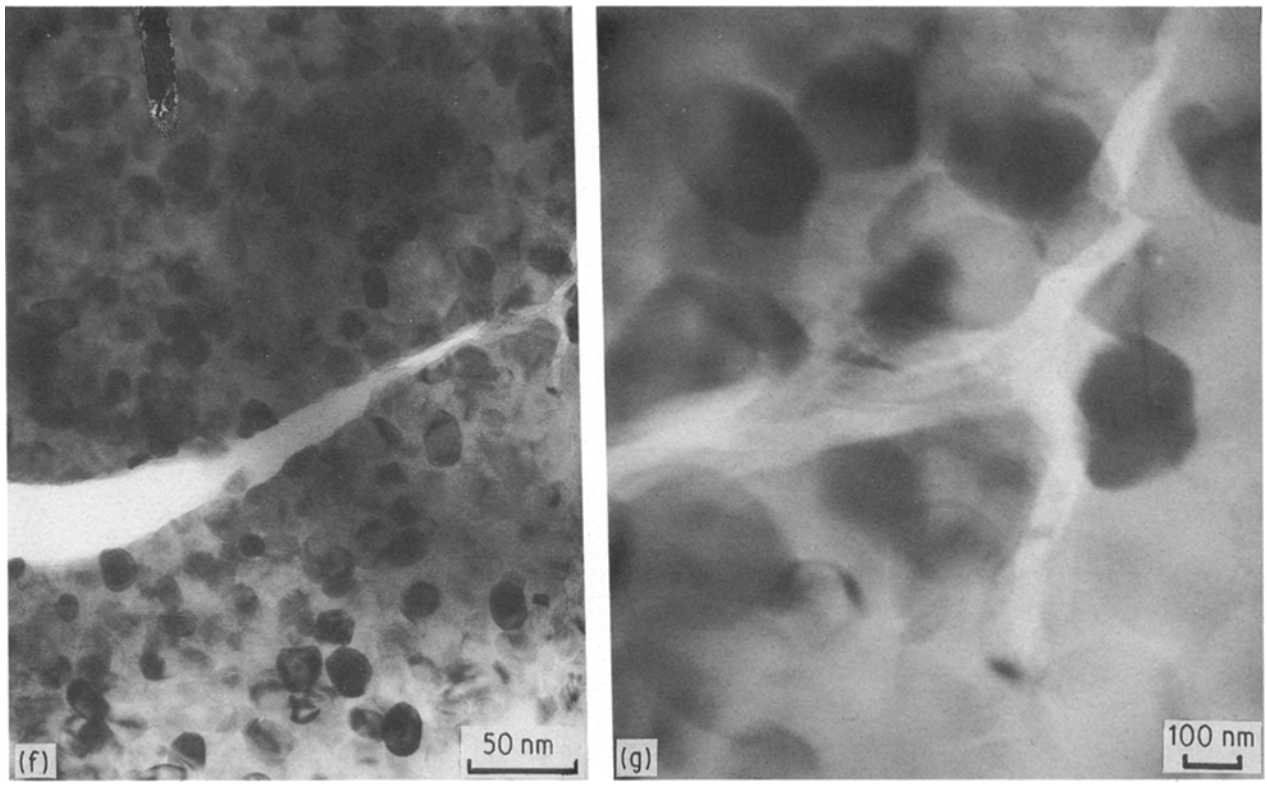

Figure 7 continued

opalescent and then white in the 1200–1300 °C temperature range, likely due to the grain size close to the visible wavelength order of magnitude (≥ 0.3 μm).

For mullite–Zr samples we simultaneously observed the transformation of tetragonal zirconia in monoclinic form and the crystallization of the mullite matrix (Fig. 4). Note that a dilatometric anomaly during the shrinkage jump can be related to the tetragonal zirconia nucleation.

The mullite–Ti material shows a more complex feature, according to the numerous DTA anomalies and the step-by-step shrinkage (Fig. 3). After the 1300 °C thermal treatment, a large part of the material remains amorphous but has a composition, deduced from EDX analysis, close to $Al_2Ti_3O_9$ (with 2% Si doping). Amorphous TiO_2 is also well visible (Fig. 6). The X-ray powder diagram is different from expected for Al_2TiO_5, but similar to that of pseudo-brookite Fe_2TiO_5 [26]. A tetragonal cell with $a = 0.95$ nm and $c = 0.358$ nm agrees with the 1030 °C X-ray powder diagram, whereas an orthorhombic cell ($a = 0.95$ nm, $b = 0.98$ nm, $c = 0.358$ nm) is more appropriate for samples heated above 1300 °C. The presence of silicon certainly plays a role in stabilizing the brookite structure. Previous studies have shown that anatase solid solution can be formed up to 20 mol % Al_2O_3 between 700 and 900 °C with sol–gel prepared materials [21].

On the other hand $(Al_xTi_{2-x})TiO_5$ solid solution with the brookite structure was usually observed by reduction and quenching [27]. Previous studies dealing with the sintering of alumina–titania powders have shown that Al_2TiO_5 is stable only above 1300 °C [12, 28]. The stability is increased if the grain size is small or if the composition is stoichiometric. Decomposition into Al_2O_3 and TiO_2 occurs at lower temperatures which can explain the rutile precipitation at the surface of samples below 1000 °C. The very high homogeneity of our way of preparation and the small size of the resulting precipitates explain the stability of the composite. The presence of organic traces in gel prepared by alkoxide hydrolysis can promote local reduction and, hence, favour formation of the $Al_2Ti_3O_9$ phase.

In our case the glassy phase remains visible at much higher temperature than is usually observed, even with previous sol–gel routes [20]. This can also be related to the very high homogeneity of mixing and to the very slow hydrolysis which avoids Al_2O_3 nucleation.

4. Fracture behaviour and mechanical properties

Fig. 8 compares typical scanning electron micrographs of fracture for pure mullite monoliths and for Ti- (or Zr-)containing monoliths. To the naked eye and at low magnification a conchoidal fracture is visible for all samples heated below 1500 °C. However, the crack propagation is complex especially when precipitates are present. A ceramic-like (inter/intragranular) fracture is only observed for samples heated for a few days at 1600 °C (Fig. 8d). Materials with glass-like fracture exhibit a precipitate size comprised between 50 nm (1050 °C thermal treatment) and 200 nm (1400 °C thermal treatment). After heating at 1600 °C, grains have a roughly cubic shape (mean size ≥ 300 nm) with a mirror plane parallel to {0 0 1} (Fig. 8d).

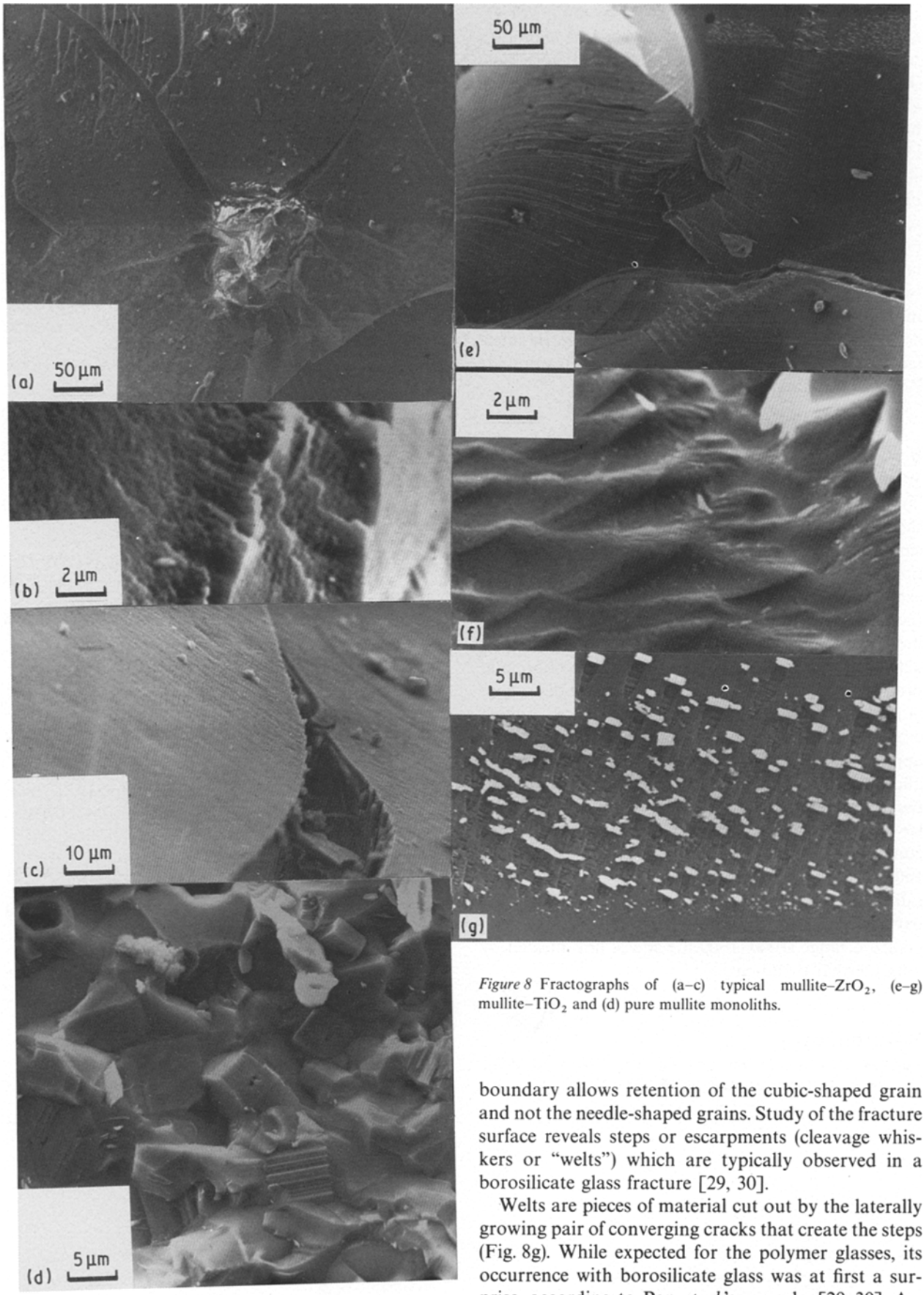

Figure 8 Fractographs of (a–c) typical mullite–ZrO_2, (e–g) mullite–TiO_2 and (d) pure mullite monoliths.

The glass-like fracture behaviour can be correlated with the remaining amorphous mullite matrix. The matrix embeds crystallized particles, which regulates and lowers the grain-growth inhibiting the Ostwald ripening. The absence of liquid phase at the grain boundary allows retention of the cubic-shaped grain and not the needle-shaped grains. Study of the fracture surface reveals steps or escarpments (cleavage whiskers or "welts") which are typically observed in a borosilicate glass fracture [29, 30].

Welts are pieces of material cut out by the laterally growing pair of converging cracks that create the steps (Fig. 8g). While expected for the polymer glasses, its occurrence with borosilicate glass was at first a surprise, according to Pan *et al.*'s remarks [29, 30]. Arrays of skewed cracks also occur in our material which shows the same "glassy" fracture. Material appears, to some extent, plastic, even so its viscosity must be very high. Skewed cracks have been previously assigned to the interaction of the crack tip with the local stress field. Thus it is easy to correlate the rugose behaviour to the presence of heterogeneities, i.e. nanoprecipitates.

Fig. 8e shows the special feature of mullite–TiO_2 samples heated at 1150 °C: the mirror face exhibits a step-by-step habit which ends with a rugose area (Fig. 8f). The picture is very similar to seracs on a glacier. It looks as if the energy fracture is adsorbed by heterogeneity when its value has become sufficiently low. However, transmission electron micrographs show that $Al_2Ti_3O_9$ precipitates induce deviation and blocking of cracks. This indicates the formation of secondary cracks as observed in a glass–epoxy composite [29, 30]. Regular marks are observed in these types of composite in relation to the interaction between primary and secondary cracks arising from initiation at the fibre interface. In our case, secondary cracks can be initiated at the precipitate–matrix interface, related to the stress-induced phase transition for ZrO_2-containing mullite.

5. Conclusion

We have shown that amorphous mullite can dissolve large amounts of Ti and Zr elements and that the addition of titanium favours low-temperature sintering. Homogeneous precipitation of nanoparticles from a refractory glassy matrix appears to be an exciting method for preparing nanocomposites. Furthermore, a toughening effect can be obtained (Fig. 7): if a fracture occurs, its propagation is stopped by a deflection of the crack in the opposite direction, and precipitate debonding. A knowledge of the phase diagram for the sol–gel prepared compositions is, however, required for designing materials for specific applications. The small size and high homogeneity allow a stable pseudo-brookite precipitate to form. In particular, it will be interesting to promote a particular nucleation at the fibre–matrix interface in order to control fibre debonding and to determine the influence of hydrolysis parameters (rate, water/alkoxide ratio) which can be modified for practical use. The particle size remains roughly stable over a large temperature range (1000–1300 °C) and is not affected by long thermal treatment.

References

1. L. C. KLEIN (Ed.), "Sol-gel Technology" (Noyes, NJ, 1988).
2. Ph. COLOMBAN, *Ceram. Int.* **15** (1989) 23–50.
3. *Idem., J. Mater. Sci.* **24** (1989) 3002.
4. *Idem., ibid.* **24** (1989) 3011.
5. *Idem.*, "Proceedings of the 2nd International Conference on Powder Science and Technology", Berchtesgaden 12–14 October 1988, edited by G. D. Messing, E. R. Fuller Jr and H. Hausner (American Ceramic Society, Westerville, Ohio, 1989) pp. 85–92.
6. Ph. COLOMBAN and L. MAZEROLLES, *J. Mater. Sci. Lett.* **9** (1990) 1077.
7. W. E. CAMERON, *Amer. Mineral.* **62** (1977) 745.
8. H. SCHNEIDER, *Ceram. Int.* **13** (1987) 77.
9. R. F. DAVIS and J. A. PASK, in "High Temperature Oxides", edited by A. M. Alper (Academic Press, 1971) pp. 37–76.
10. S. PROCHAZKA, J. S. WALLACE and N. CLAUSSEN, *J. Amer. Ceram. Soc.* **66** (1983) C. 125.
11. A. MAKISHIMA, H. OOSHASKI, M. WAKAKAWA, T. SHIMOHIRA and K. KOTAMI, *J. Non-Cryst. Solids* **42** (1980) 545.
12. H. OKAMURA, E. A. BARRINGER and H. K. BOWEN, *J. Mater. Sci.* **24** (1989) 1867.
13. Ph. COLOMBAN, "Ceramics Today, Tomorrow's Ceramics", edited by P. Vincenzini (Elsevier) to be published.
14. I. M. LOW and R. McPHERSON, *J. Mater. Sci.* **24** (1989) 926.
15. *Idem., ibid.* **24** (1989) 951.
16. K. OKADA and N. OTSUKA, *J. Amer. Ceram. Soc.* **69** (1986) 652.
17. *Idem., Sci. Ceram.* **14** (1989) 497.
18. S. SEN and S. THIAGARAJAN, *Ceram. Int.* **14** (1988) 77.
19. P. McMILLAN and B. PIRIOU, *J. Non-Cryst. Solids* **53** (1982) 279.
20. I. W. BROWN, K. J. D. McKENZIE, M. E. BOWDEN and R. H. MEINHOLD, *J. Amer. Ceram. Soc.* **68** (1985) 298.
21. O. YAMAGUCHI and Y. MUKAIDA, *ibid.* **72** (1989) 330.
22. H. KNOLL, *Naturwiss.* **48** (1961) 601.
23. S. P. S. PORTO, P. A. FLEURY and T. C. DAMEN, *Phys. Rev.* **154** (1964) 522.
24. U. BALACHANDRAN and N. G. EROR, *J. Solid State Chem.* **42** (1982) 276.
25. C. A. MELENDRES, A. NARAYANASMI, V. A. MARONI and R. W. SIEGEL, *J. Mater. Res.* **4** (1989) 1246.
26. International Centre for Diffraction Data no. 9-182 ($FeTiO_5$) and 26-40 (Al_2TiO_5).
27. D. GOLDBERG, Thesis, Paris (1968).
28. P. A. BRUGGER and A. MOCELLIN, *J. Mater. Sci.* **21** (1986) 4431.
29. T. Y. PAN, R. E. ROBERTSON and F. E. FILISKO, *ibid.* **23** (1988) 2553.
30. *Idem., ibid.* **24** (1989) 3635.

Received 23 April
and accepted 4 September 1990